

Atomic structure of the two intermediate phase glasses SiSe₄ and GeSe₄Carlo Massobrio,¹ Massimo Celino,² Philip S. Salmon,³ Richard A. Martin,³ Matthieu Micoulaut,⁴ and Alfredo Pasquarello^{5,6}¹*Institut de Physique et de Chimie des Matériaux de Strasbourg, 23 rue du Loess, BP43, F-67034 Strasbourg Cedex 2, France*²*ENEA, Ente per le Nuove Tecnologie, l'Energia e l'Ambiente, Unità Materiali e Nuove Tecnologie,**C.R. Casaccia, CP 2400, 00100 Roma, Italy*³*Department of Physics, University of Bath, Bath BA2 7AY, United Kingdom*⁴*Laboratoire de Physique Théorique des Liquids, Université Pierre et Marie Curie, 4 Place Jussieu, F-75252 Paris Cedex 05, France*⁵*Institute of Theoretical Physics, Ecole Polytechnique Fédérale de Lausanne (EPFL), CH-1015 Lausanne, Switzerland*⁶*Institut Romand de Recherche Numérique en Physique des Matériaux (IRRMA), CH-1015 Lausanne, Switzerland*

(Received 8 September 2008; revised manuscript received 17 February 2009; published 4 May 2009)

The microscopic origin of the intermediate phase in two prototypical covalently bonded A_xB_{1-x} network glass forming systems, where $A=Ge$ or Si , $B=Se$, and $0 \leq x \leq 1$, was investigated by combining neutron diffraction with first-principles molecular-dynamics methods. Specifically, the structure of glassy $GeSe_4$ and $SiSe_4$ was examined, and the calculated total structure factor and total pair-correlation function for both materials are in good agreement with experiment. The structure of both glasses differs markedly from a simple model comprising undefective AB_4 corner-sharing tetrahedra in which all A atoms are linked by B_2 dimers. Instead, edge-sharing tetrahedra occur and the twofold coordinated Se atoms form three distinct structural motifs, namely, $Se-Se_2$, $Se-SeGe$ (or $Se-SeSi$), and $Se-Ge_2$ (or $Se-Si_2$). This identifies several of the conformations that are responsible for the structural variability in Ge_xSe_{1-x} and Si_xSe_{1-x} glasses, a quantity that is linked to the finite width of the intermediate phase window.

DOI: 10.1103/PhysRevB.79.174201

PACS number(s): 61.43.Fs

I. INTRODUCTION

Network forming glasses are characterized by a threshold which marks a transition in their physical properties around a mean coordination number $\bar{n} \approx 2.4$.^{1,2} This threshold is the consequence of structural modifications driven by a variation in the system composition, the character of which is not fully understood. Chalcogenide glasses from the A_xB_{1-x} family ($A=Si, Ge; B=S, Se$ with $0 \leq x \leq 1$) exhibit this phenomenon around $x=0.2$ and there is a wealth of experimental information on the composition dependence of the system properties.¹⁻¹⁷ These materials are therefore excellent candidates for providing information that will help to elucidate the atomic-scale nature of the transition.

According to early theoretical approaches, the threshold is defined by an equality between the number of bonding constraints per atom and the number of degrees of freedom, marking the change from an elastically floppy or underconstrained network to a stressed-rigid or overconstrained network.^{18,19} The existence of a single elastic phase transition in these materials has, however, been challenged by the results obtained from more recent spectroscopic and calorimetric experiments showing a finite interval of compositions around $x=0.2$ which demarcates between the floppy and stressed-rigid regimes.³⁻⁷ This composition window is associated with a so-called intermediate phase (IP) where the network is deemed to self-organize on formation to give a rigid system that is optimally constrained to avoid stress.²⁰ Generic models that contain no specific information on the chemical nature of the constituents are able to reproduce a double transition in the network properties.²¹⁻²³ More recently, the width of the IP has been rationalized by introducing the notion of *structural variability*.²³ This concept can be illustrated by referring to a representative subset of A and B

atoms in the case of an AB_4 system such as $GeSe_4$, a snapshot of which is illustrated in Fig. 1. The neighborhood of a twofold coordinated B atom consists of either (a) two B neighbors, (b) one B and one A neighbor, or (c) two A neighbors, configurations that are labeled as BB , AB , and AA , respectively. For a system of undefective AB_4 corner-sharing tetrahedra in which all A atoms are connected by B_2 dimers, the fractions of AA , BB , and AB units are 0%, 0%, and 100%, respectively. This corresponds to a chemically ordered network^{11,17,24} with no intermediate phase, i.e., to a vanishing intermediate phase window which allows for only a single elastic transition (from floppy to stressed rigid), as predicted in Ref. 23. The extent of departure from a network containing 100% AB units (hereafter termed a “full AB ” network) is called structural variability to indicate the different conformations that allow for self-organization in the interme-

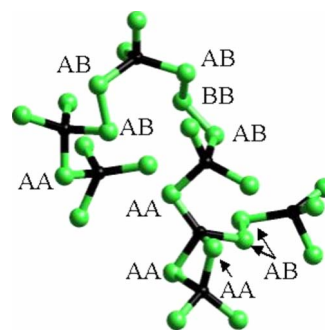


FIG. 1. (Color online) A representative subset of Ge and Se atoms in amorphous $GeSe_4$ where Ge atoms are dark (black) and Se atoms are light (green). Se atoms along a connection path between two Ge atoms are labeled as AA , those between one Ge atom and one Se atom are labeled as AB , and those between two Se atoms are labeled as BB .

diate phase.²³ The width of the intermediate phase for an A_xB_{1-x} material is related to the structural variability, a larger variability leading to a wider range of IP compositions.

In this paper we investigate the structural variability and hence the origin of the intermediate phase window in network glasses by using an approach based on neutron-diffraction experiments and first-principles molecular-dynamics (FPMD) simulations within density-functional theory, both performed on glassy GeSe_4 ($g\text{-GeSe}_4$) and glassy SiSe_4 ($g\text{-SiSe}_4$). First, our FPMD models are validated via a comparison with the neutron-diffraction data, showing very good agreement between experiment and theory for both the total structure factor and the total pair-correlation function. Then we examine the departure from a full AB network, which is due to a rich variety of Se bonding configurations and edge-sharing tetrahedral connections, and find that this departure is larger in the case of $g\text{-SiSe}_4$. Spectroscopic and calorimetric experiments suggest that the width of the IP window is marginally larger for $\text{Si}_x\text{Se}_{1-x}$ compared to $\text{Ge}_x\text{Se}_{1-x}$.^{4,8,9} Our results thereby provide a quantitative atomic-scale counterpart to the findings of Ref. 23 where generic models are used to provide a link between structural variability and the finite width of the IP window.

The paper is organized as follows. The experimental setup and the theoretical model are outlined in Secs. II and III, respectively. The results are then presented in Sec. IV in four distinct subsections. In the first, we focus on a comparison between the measured and calculated total structure factors, and total pair-correlation functions for glassy GeSe_4 and SiSe_4 . In the second, the calculated partial structure factors for both materials are compared, and, in the third, the corresponding pair-correlation functions and bond-angle distributions are considered. In the fourth, we describe in more detail the features of the glassy GeSe_4 and SiSe_4 networks, and hence quantify their structural variability. Concluding remarks are given in Sec. V.

II. EXPERIMENTAL SETUP

The SiSe_4 glass was prepared from Si (99.9999%) and Se (99.999%) by quenching the liquid, mixed at 1100 °C for ≈ 2 days in a silica ampoule of 7 mm inner diameter and 1 mm wall thickness, from 870 °C in an ice/salt-water mixture. The neutron-diffraction experiment for $g\text{-SiSe}_4$ was made using the GEneral Materials (GEM) diffractometer at the ISIS pulsed neutron source.²⁵ In this experiment, diffraction patterns were measured for a coarsely ground SiSe_4 powder in a vanadium container with inner diameter of 4.8 mm and wall thickness of 0.1 mm at ambient temperature (≈ 25 °C), the empty vanadium container, the empty instrument, and a vanadium rod with diameter of 6 mm for normalization purposes. The data were analyzed using the program GUDRUN,²⁶ which makes the necessary corrections detector by detector before merging the results to give the total structure factor $S_T(k)$. The diffraction experiment for $g\text{-GeSe}_4$ is described by Petri and Salmon.¹¹ The reliability checks made on the data sets are described elsewhere.²⁷ The atomic number densities are $0.0331(2)$ Å⁻³ for $g\text{-SiSe}_4$ (Ref. 14) and $0.0339(1)$ Å⁻³ for $g\text{-GeSe}_4$.¹¹

III. THEORETICAL MODEL

Systems of 24 Ge and 96 Se (GeSe_4) or 24 Si and 96 Se (SiSe_4) atoms were simulated in the number, volume, temperature (NVT) ensemble.^{28,29} Periodically repeated cubic cells of length 15.38 Å ($g\text{-SiSe}_4$) or 15.27 Å ($g\text{-GeSe}_4$) were adopted, corresponding to the experimental densities at a temperature $T=300$ K. The system size allows coverage of the region $k \leq 1$ Å⁻¹ by as many as seven discrete wave vectors compatible with the periodicity of the supercells. This ensures a precise description of the ordering at intermediate range distances, well beyond the first shell of neighbors. A self-consistent evolution of the electronic structure was described by using density-functional theory where a generalized gradient approximation (GGA) was adopted for the exchange and correlation parts of the total energy.³⁰ The valence electrons were treated explicitly whereas norm conserving pseudopotentials were used to account for the core-valence interactions. The pseudopotentials for Ge, Se, and Si were generated as in Ref. 31. The wave functions were expanded in plane waves at the Γ point of the supercell and the energy cutoff was taken to be $E_c=20$ Ry. Other technical features are extensively described in our previous work on liquid and glassy GeSe_2 (Refs. 32–36), liquid GeSe_4 (Ref. 24), and amorphous SiSe_2 .³⁷

In the case of GeSe_4 we first extended a temporal trajectory, previously generated for the liquid at $T=1073$ K, up to 20 ps.²⁴ Then $N_{\text{st}}=5$ configurations separated by 3 ps were selected to provide starting sets of coordinates. These initial configurations are uncorrelated since their time separation (3 ps) is much longer than the decay time (less than 1 ps, see Fig. 1 of Ref. 24) of the single-particle velocity-velocity self-correlation function. For each initial set, and after rescaling the coordinates to match the density of the glass, the system was first cooled down to $T=600$ K in 12 ps and then quenched and further annealed for 8 ps at $T=300$ K. Data were collected over a period of 6 ps for each of these N_{st} subtrajectories. Glassy SiSe_4 was prepared from an initial random configuration at $T=1600$ K by cooling the system to $T=300$ K in 25 ps and then selecting $N_{\text{st}}=4$ configurations separated by ~ 4 ps. Data were collected over periods of 4 ps for each of these N_{st} subtrajectories. For both $g\text{-GeSe}_4$ and $g\text{-SiSe}_4$, overall mean values and error bars were extracted from the partial averages provided by each subtrajectory.

It should be noted that the choice of cell size to reproduce the glass density does not predetermine either the bond distances or the nearest-neighbor coordination environment of the atoms. Instead, these quantities are much more sensitive to the accuracy of the scheme used to describe the chemical bonding and, in particular, to the exchange-correlation part of the total energy. We refer to a study on the nature of the bonding in liquid GeSe_2 for an instructive example of the role played by a generalized gradient approximation in improving the structural description beyond that achievable with a local-density approximation.³³

The method employed to prepare each glass is a compromise between use of the FPMD method to provide an accurate description of the chemical bonding and the limited temporal span of FPMD trajectories which leads to high quench

rates. Nevertheless, this approach has an extensive record of reliability for an extended set of disordered chalcogenide systems characterized by a high degree of chemical order, as shown by a comparison with measured structural properties such as the total and partial pair-correlation functions, and the total and partial structure factors.^{24,32–37} A satisfactory level of agreement has also been found between FPMD and experiment for the vibrational properties of glassy GeSe₂ by considering a single configuration optimized at $T=0$ K.³⁸ In the case of g -GeSe₂, the impact of relaxation on the structural properties has been investigated in detail.³⁶ It is found that, by taking trajectories for several uncorrelated starting liquid state configurations and by annealing the system at the target temperature for intervals of the order ≈ 10 ps, a substantial change in the structure is observed, i.e., memory of the starting liquid can be effectively minimized. In the case of GeSe₂, the main effect of a quench from the liquid is to restore chemical order by reducing the number of miscoordinations and homopolar bonds.³⁶ This effect also occurred for the GeSe₄ and SiSe₄ systems investigated in the present work but the observed changes were not so pronounced since the starting liquids showed smaller deviations from chemical order. A relative similarity between the liquid and glass structures for systems such as GeSe₄ might be anticipated from the relative difficulty of glass formation in the Ge_xSe_{1-x} system which takes a maximum for $x=0.33$ and has minimal values for $x=0.1-0.2$.³⁹ In summary, one has to be aware that different quench rates may alter the relative proportions of the various structural units in the glass. However, at least in the case of GeSe₄ and SiSe₄, the identity of these units is not expected to be drastically different when moving from the liquid to the glass. The results given in Sec. IV D on the nature of the Se coordination environment in liquid (see Ref. 24) and glassy GeSe₄ support this statement.

It is notable that another molecular-dynamics approach has been used to investigate Ge_xSe_{1-x} glasses near the intermediate phase.⁴⁰ In this work, the molecular-dynamics calculations were made by using a nonself-consistent electronic structure scheme based on the local-density approximation of density-functional theory and a minimal basis set. It was suggested that a change with composition in several structural features might be a signature of the IP, in particular the number of twofold coordinated Se units containing neighbors of a different atomic type. X-ray diffraction studies of Ge_xSe_{1-x} glasses showed some evidence for a structural origin to the intermediate phase from the composition dependence of the properties of the first-sharp diffraction peak (FSDP) in the measured total structure factors.^{15,16} These findings were not, however, confirmed by more recent x-ray diffraction work which did not reveal any discontinuities in the structural parameters that could clearly be attributed to the intermediate phase.¹⁰

IV. RESULTS

A. Neutron total structure factors and total pair-correlation functions

The calculated total structure factors $S_T(k)$ for g -GeSe₄ and g -SiSe₄ show very good agreement with the correspond-

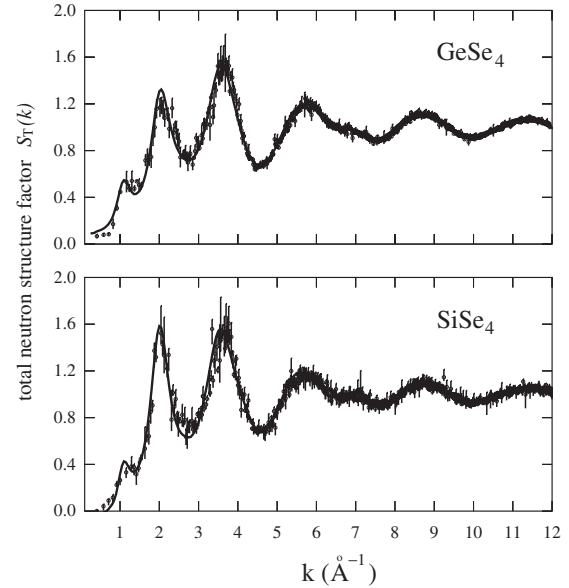


FIG. 2. The measured (full curve) and calculated (dots with error bars) total neutron structure factors $S_T(k)$ for glassy GeSe₄ (upper panel) and glassy SiSe₄ (lower panel). The coherent neutron-scattering lengths are $b_{\text{Si}}=4.1491$ fm, $b_{\text{Se}}=7.970$ fm, and $b_{\text{Ge}}=8.185$ fm. The first-sharp diffraction peak in the measured $S_T(k)$ appears at $k=1.12(2)$ Å⁻¹ for g -GeSe₄ and at $k=1.14(2)$ Å⁻¹ for g -SiSe₄.

ing neutron-diffraction data (Fig. 2). For $k \geq 2$ Å⁻¹, the peak positions and intensities are well reproduced within the statistical error. Around $k=1$ Å⁻¹, the first-sharp diffraction peak is slightly less pronounced, taking the form of a bump. Note that the larger noise in the modeled $S_T(k)$ for g -SiSe₄ is due to poorer statistics. In Fig. 3(a), the calculated and experimental total pair-correlation functions are compared for g -GeSe₄. On the experimental side, $g_T^{\text{exp}}(r)$ was obtained by Fourier transforming the reciprocal space data set with an upper limit of integration $k_{\text{max}}=15.95$ Å⁻¹ which results from the finite measurement window function of the diffractometer and which leads to spurious oscillations at $r < 2$ Å. When the same approach is applied to the calculated $S_T(k)$, the resulting total pair-correlation function $g_T^{\text{th}(b)}(r)$ is found to reproduce $g_T^{\text{exp}}(r)$ over the entire range. The FPMD total pair-correlation function obtained directly from the atomic coordinates, $g_T^{\text{th}}(r)$, has a sharper main peak. In the case of g -SiSe₄ [Fig. 3(b)], the neutron-diffraction data were taken over a much larger interval which extended to $k_{\text{max}}=40$ Å⁻¹. Despite a small residual difference in the peak intensities, $g_T^{\text{exp}}(r)$ and $g_T^{\text{th}}(r)$ are in overall agreement.

B. Partial structure factors

In Fig. 4 we compare the calculated Faber-Ziman partial structure factors $S_{\text{SeSe}}(k)$, $S_{\text{ASe}}(k)$, and $S_{\text{AA}}(k)$, where A denotes Ge or Si, for g -GeSe₄ and g -SiSe₄. The corresponding $S_{\text{SeSe}}(k)$ and $S_{\text{ASe}}(k)$ functions for both glasses are remarkably similar, showing comparable peak positions and intensities. The $S_{\text{AA}}(k)$ functions have a larger statistical noise owing to a smaller fraction of A atoms at the ASE₄ stoichi-

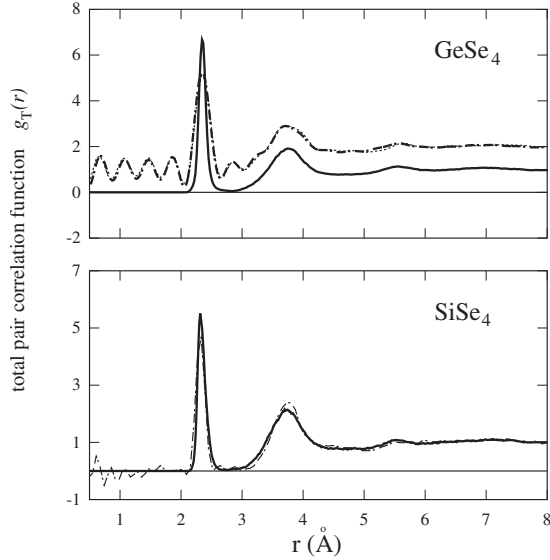


FIG. 3. (a) Upper panel: total pair-correlation function for GeSe_4 . The dash-dotted curve gives the measured $g_T^{\text{exp}}(r)$ obtained by Fourier transforming the measured $S_T(k)$ function with a cutoff value $k_{\text{max}}=15.95 \text{ \AA}^{-1}$, the dotted curve gives the FPMD $g_T^{\text{th(b)}}(r)$ obtained from the simulated $S_T(k)$ function by applying the same procedure, and the full curve gives the FPMD $g_T^{\text{th}}(r)$ obtained by direct calculation from the real-space coordinates. Note that $g_T^{\text{exp}}(r)$ and $g_T^{\text{th(b)}}(r)$ are essentially identical and, for clarity of presentation, have been displaced upward by adding a constant of unity. The first peak in $g_T^{\text{exp}}(r)$ occurs at $r_1=2.35(2) \text{ \AA}$ and the ratio of the first two peak positions $r_2/r_1=1.583$. (b) Lower panel: total pair-correlation function for SiSe_4 . The dash-dotted curve gives the measured $g_T^{\text{exp}}(r)$ obtained by Fourier transforming the measured $S_T(k)$ function with $k_{\text{max}}=40 \text{ \AA}^{-1}$ and the full curve gives the FPMD $g_T^{\text{th}}(r)$ obtained by direct calculation from the real-space coordinates. For $g_T^{\text{exp}}(r)$, $r_1=2.32(1) \text{ \AA}$ and $r_2/r_1=1.625$.

ometry and, in the case of $g\text{-SiSe}_4$, due to the employment of shorter temporal trajectories. Although the $A\text{-A}$ partial structure factors show spurious spikes, their shapes also follow the same trend with a distinct feature occurring in the region of the FSDP at $k \approx 1 \text{ \AA}^{-1}$. For both systems, an FSDP is also clearly detectable in $S_{A\text{Se}}(k)$ but is absent in $S_{\text{SeSe}}(k)$. These observations for the FSDP compare with anomalous x-ray scattering results for glassy $\text{Ge}_x\text{Se}_{1-x}$ with $x=0.195$ and $x=0.23$ which suggest a dominant contribution to the FSDP from Ge-Ge correlations.^{12,13} In the case of liquid and glassy GeSe_2 , the measured partial structure factors show a dominant contribution to the FSDP from Ge-Ge correlations with a non-negligible contribution from Ge-Se correlations.⁴¹⁻⁴³

In Fig. 5 we focus on the calculated Bhatia-Thornton concentration-concentration partial structure factor $S_{\text{CC}}(k)$.^{44,45} This partial structure factor can be obtained from a linear combination of the Faber-Ziman partial structure factors and takes the form

$$S_{\text{CC}}(k) = c_A c_B \{ 1 + c_A c_B [S_{AA}(k) - S_{AB}(k)] + [S_{BB}(k) - S_{AB}(k)] \}, \quad (1)$$

where c_α is the atomic fraction of chemical species α . $S_{\text{CC}}(k)$ is sensitive to chemical disorder since it reflects the chemical

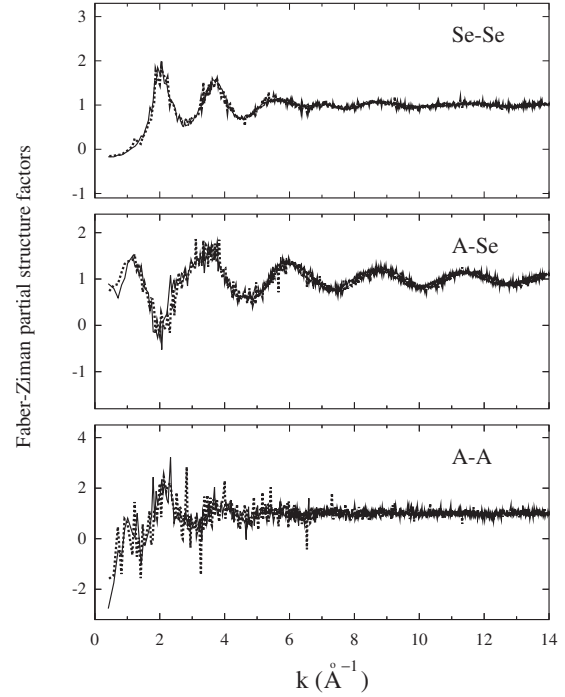


FIG. 4. The calculated Faber-Ziman partial structure factors for glassy GeSe_4 (solid curves) and glassy SiSe_4 (dotted curves). The label Se-Se indicates $S_{\text{SeSe}}(k)$, the label A-Se indicates either $S_{\text{GeSe}}(k)$ or $S_{\text{SiSe}}(k)$, and the label A-A indicates either $S_{\text{GeGe}}(k)$ or $S_{\text{SiSi}}(k)$.

environment of each atom.⁴⁶ The very similar shapes of the $S_{\text{CC}}(k)$ partial structure factors for $g\text{-GeSe}_4$ and $g\text{-SiSe}_4$ stems from the similarities between the two sets of Faber-Ziman partial structure factors mentioned above. In particular, there is a small feature in the region of the FSDP which may be interpreted by reference to the results obtained from first-principles molecular-dynamics simulations for a series of liquids and glasses.⁴⁷ It was shown that a distinct feature appears in $S_{\text{CC}}(k)$ at the location of the FSDP when there is a moderate departure from chemical order but that this feature vanishes when there is a high level of chemical disorder or when the chemical order is essentially perfect.⁴⁷ The calculated $S_{\text{CC}}(k)$ functions for $g\text{-GeSe}_4$ and $g\text{-SiSe}_4$ therefore suggest a moderate amount of chemical disorder in both systems. This picture for the structural organization is supported by the results given in Sec. IV D which show a small depar-

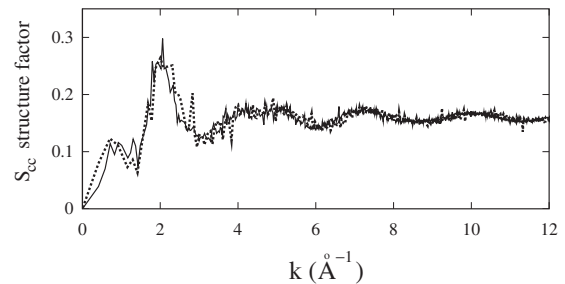


FIG. 5. The calculated Bhatia-Thornton concentration-concentration partial structure factor $S_{\text{CC}}(k)$ for glassy GeSe_4 (solid curve) and glassy SiSe_4 (dotted curve).

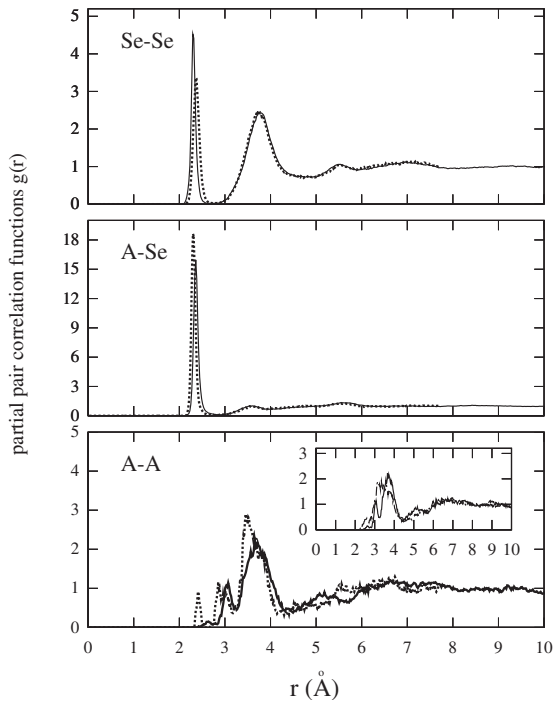


FIG. 6. The calculated partial pair-correlation functions for glassy GeSe_4 (solid curves) and glassy SiSe_4 (dotted curves). The label Se-Se indicates $g_{\text{SeSe}}(r)$, the label A-Se indicates either $g_{\text{GeSe}}(r)$ or $g_{\text{SiSe}}(r)$, and the label A-A indicates either $g_{\text{GeGe}}(r)$ or $g_{\text{SiSi}}(r)$. Inset: comparison between the calculated partial pair-correlation function $g_{\text{GeGe}}(r)$ for glassy GeSe_4 (solid curve) and the calculated partial pair-correlation function $g_{\text{GeGe}}(r)$ for liquid GeSe_4 (dash-dotted curve) from Ref. 24.

ture from a chemically ordered network model in which the A-Se coordination number is four and Se is twofold coordinated.²⁴

C. Pair-correlation functions and bond-angle distributions

In Fig. 6 we display the calculated partial pair-correlation functions $g_{\text{SeSe}}(r)$, $g_{\text{ASe}}(r)$, and $g_{\text{AA}}(r)$ for both $g\text{-GeSe}_4$ and $g\text{-SiSe}_4$. The first peak in $g_{\text{SeSe}}(r)$ is indicative of Se-Se homopolar bonds, with slightly shorter distances occurring in the case of $g\text{-GeSe}_4$. For $r > 3$ Å the $g_{\text{SeSe}}(r)$ functions are essentially identical, pointing toward a similar organization of the Se subnetworks. The first peak in both $g_{\text{GeSe}}(r)$ and $g_{\text{SiSe}}(r)$ is relatively sharp, and can be ascribed to the predominance of GeSe_4 or SiSe_4 tetrahedral units.

The comparison between $g_{\text{GeGe}}(r)$ and $g_{\text{SiSi}}(r)$ shows the existence of three distinct features in the region $2 \lesssim r(\text{Å}) \lesssim 4$. With increasing r , these features can be identified with homopolar Ge-Ge or Si-Si bonds, Ge or Si atoms involved in edge-sharing tetrahedral connections, and Ge or Si atoms involved in corner-sharing tetrahedral connections, respectively. The features are more clearly separated in the case of $g\text{-SiSe}_4$ which has a larger number of Si-Si homopolar bonds. In Fig. 6 $g_{\text{GeGe}}(r)$ for the glass is also compared with the calculated pair-correlation function for liquid GeSe_4 .²⁴ It is evident that the shape of $g_{\text{GeGe}}(r)$ undergoes a dramatic change upon cooling, particularly for distances in the range

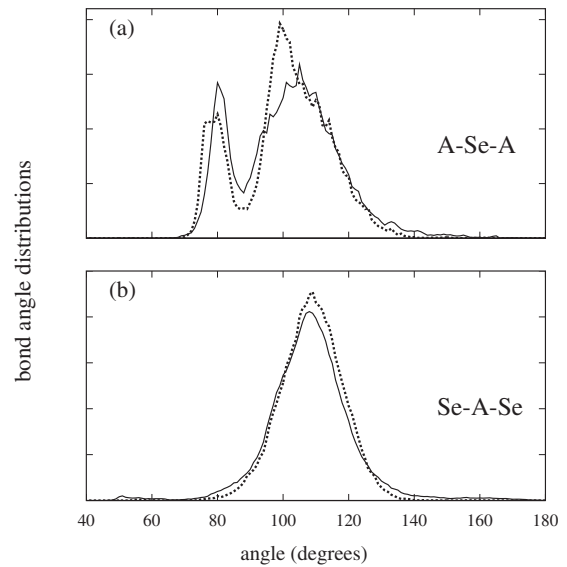


FIG. 7. The calculated bond-angle distributions for glassy GeSe_4 (solid curves) and glassy SiSe_4 (dotted curves). The label A-Se-A indicates either the Ge-Se-Ge or Si-Se-Si bond-angle distribution while the label Se-A-Se indicates either the Se-Ge-Se or Se-Si-Se bond-angle distribution.

$3 \lesssim r(\text{Å}) \lesssim 4$, where only a broad peak is observable for the molten phase. The method we used to quench the liquid into a glass has therefore led to significant differences between the corresponding pair-correlation functions. The clear separation between three distinct classes of Ge-Ge or Si-Si neighbors (belonging to homopolar, corner-sharing, and edge-sharing connections) is a typical fingerprint of the structure of glassy chalcogenides, as shown in detail for the case of amorphous GeSe_2 .^{36,43}

In Fig. 7 we show the Se-A-Se (θ_{SeASe}) and A-Se-A (θ_{ASeA}) bond-angle distributions for $g\text{-GeSe}_4$ and $g\text{-SiSe}_4$. These distribution functions have been calculated by including neighbors separated by less than 3 Å. Two main peaks appear in the A-Se-A bond-angle distributions and, by analogy with the analysis carried out for amorphous GeSe_2 ,³⁶ their structural origin can be readily identified. The first peak is ascribed to edge-sharing tetrahedra, i.e., to Ge or Si centered subunits which have in common two Se atoms, while the second peak is attributed to corner-sharing tetrahedra which share only a single Se atom. The main peaks in θ_{SiSeSi} for $g\text{-SiSe}_4$ appear at 80° and 99° . By comparison, the first peak in θ_{GeSeGe} for $g\text{-GeSe}_4$ also occurs at 80° but has a higher intensity while the second peak is broader and of lower intensity, with a maximum at 105° . The profiles of the Se-Ge-Se and Se-Si-Se bond-angle distributions are symmetrical about a maximum at 109° , as expected for a tetrahedral network with a very small number of coordination defects, which reflect the predominant fourfold coordination environments of the Ge and Si atoms. A contrast is provided by the Se-Ge-Se bond-angle distribution for liquid GeSe (see Fig. 6 of Ref. 48) in which there is a wide variety of structural motifs.^{48,49}

D. Structural variability of the intermediate phase glasses

The family of glassy systems $\text{Ge}_x\text{Se}_{1-x}$ and $\text{Si}_x\text{Se}_{1-x}$ is characterized by finite widths for the corresponding interme-

diate phase windows, as shown by Raman spectroscopy and modulated differential scanning calorimetry measurements. For example, the IP window indicated by the variation in Raman mode frequency for corner- or edge-sharing tetrahedra extends over the x value range of 0.190(5)–0.265(5) or 0.170(5)–0.265(5), respectively, for $\text{Si}_x\text{Se}_{1-x}$ (see Fig. 17 of Ref. 4), and over the reduced range of 0.220(5)–0.255(5) or 0.200(5)–0.265(5), respectively, for $\text{Ge}_x\text{Se}_{1-x}$ (see Fig. 3 of Ref. 8). These results give a mean composition range of $0.18(1) < x < 0.265(5)$ for $\text{Si}_x\text{Se}_{1-x}$, which corresponds to a spread in average coordination number $\Delta\bar{n}=0.17 \pm 0.04$ where $\bar{n}=2(1+x)$, together with a mean composition range of $0.21(1) < x < 0.26(1)$ for $\text{Ge}_x\text{Se}_{1-x}$, which corresponds to $\Delta\bar{n}=0.10 \pm 0.06$. By comparison, the nonreversing heat flow ΔH_{nr} obtained from the calorimetry experiments indicates an x value range of 0.20(1)–0.275(5) for $\text{Si}_x\text{Se}_{1-x}$ (Ref. 4) or 0.20(1)–0.26(1) for $\text{Ge}_x\text{Se}_{1-x}$ (Ref. 8). These small but systematic trends indicate an IP window that is slightly wider for the glassy $\text{Si}_x\text{Se}_{1-x}$ system. Based on the qualitative predictions of Ref. 23, the finite widths call for networks featuring non-negligible amounts of *AA* and *BB* configurations in both systems (see Fig. 1). Also, a larger width for the $\text{Si}_x\text{Se}_{1-x}$ system compared to $\text{Ge}_x\text{Se}_{1-x}$ would call for a larger structural variability.

The atomic structure of $g\text{-GeSe}_4$ and $g\text{-SiSe}_4$ can be described in terms of the fractions of *A* (Ge or Si) and *Se* centered structural motifs (see Table I). In both glasses, the number of Se-Se homopolar bonds is fairly large, involving 73% of the Se atoms in $g\text{-GeSe}_4$ and 72% of the Se atoms in $g\text{-SiSe}_4$. These bonds interconnect GeSe_4 or SiSe_4 tetrahedra in which 88% of the Ge atoms or 89% of the Si atoms are involved (see Table I). A few Ge (or Si) atoms are not fourfold coordinated to Se atoms but form Ge-Se₂ (or Si-Se₂), Ge-Se₃ (or Si-Se₃), and Ge-GeSe₃ (or Si-SiSe₃) units. Our model for glassy GeSe_4 is more chemically ordered than that obtained by Tafen and Drabold⁵⁰ where 77% of the Ge atoms are involved in GeSe_4 tetrahedra. Chains of Se atoms are found in both $g\text{-GeSe}_4$ and $g\text{-SiSe}_4$, i.e., in addition to the predominant dimer subunit, trimers and tetramers also occur. As shown in Table I, 26% of the Se atoms in $g\text{-GeSe}_4$ and 30% of the Se atoms in $g\text{-SiSe}_4$ have at least two Se atoms as nearest neighbors.

An analysis of the Se conformations helps to illustrate the way in which the Se atoms crosslink Ge or Si centered motifs (see Table I) where the *AA*, *BB*, and *AB* notations are used to classify the neighborhood of twofold coordinated Se atoms (see Fig. 1). Both systems are found to depart significantly from the full *AB* network for which the fractions of *AA*, *BB*, and *AB* units are 0%, 0%, and 100%, respectively. In both cases *AB* units predominate, with 47% in $g\text{-GeSe}_4$ and 42% in $g\text{-SiSe}_4$, but *AA* and *BB* units are far from negligible, with 23% of *AA* units in $g\text{-GeSe}_4$ and 25% in $g\text{-SiSe}_4$, and with 26% of *BB* units in $g\text{-GeSe}_4$ and 30% in $g\text{-SiSe}_4$. In the case of GeSe_4 , the fractions of *AA*, *BB*, and *AB* units recorded for the glass compare with liquid state values of 30%, 30%, and 40%, respectively (see Ref. 24). Similar percentages have also been found for liquid SiSe_4 .

The conformations in $g\text{-GeSe}_4$ and $g\text{-SiSe}_4$ that account for the structural variability, which is held responsible for the finite width of the intermediate phase window in the corre-

TABLE I. Upper part: the fraction (in percent) of Ge and Se centered structural motifs in glassy GeSe_4 , and of Si and Se centered structural motifs in glassy SiSe_4 . The first symbol defines the atom at the center of a structural motif while symbols after the dash identify the nearest neighbors within a cutoff distance of 2.7 Å. For instance, Ge-GeSe₃ means a fourfold coordinated Ge with one Ge and three Se nearest neighbors. Structural motifs accounting for less than 1% of Ge or Si atoms are not reported. Note that the Se-Se₂, Se-SeGe (Se-SeSi), and Se-Ge₂ (Se-Si₂) conformations have been labeled as *BB*, *AB*, and *AA*, respectively. Lower part: the fraction (in percent) of Ge(Si) atoms forming edge-sharing tetrahedra, $N_{\text{Ge(Si)}}(\text{ES})$, the fraction of Ge(Si) atoms forming corner-sharing tetrahedra, $N_{\text{Ge(Si)}}(\text{CS})$, the fraction of Ge or Si atoms involved in homopolar bonds, $N_{\text{Ge-Ge}}$ or $N_{\text{Si-Si}}$, and the fraction of Se atoms involved in homopolar bonds, $N_{\text{Se-Se}}$.

<hr/> <hr/>			
GeSe_4			
Ge-Se ₂	4 ± 1	Se-Se ₂ (<i>BB</i>)	26 ± 1
Ge-Se ₃	4 ± 1	Se-SeGe (<i>AB</i>)	47 ± 1
Ge-GeSe ₃	2 ± 1	Se-Ge ₂ (<i>AA</i>)	23 ± 1
Ge-Se ₄	88 ± 2		
<hr/>			
SiSe_4			
Si-Se ₂	3 ± 1	Se-Se ₂ (<i>BB</i>)	30 ± 1
Si-Se ₃	4 ± 1	Se-SeSi (<i>AB</i>)	42 ± 1
Si-SiSe ₃	4 ± 1	Se-Si ₂ (<i>AA</i>)	25 ± 1
Si-Se ₄	89 ± 2		
<hr/>			
GeSe_4			
$N_{\text{Ge}}(\text{ES})$	$N_{\text{Ge}}(\text{CS})$	$N_{\text{Ge-Ge}}$	$N_{\text{Se-Se}}$
22 ± 4	75 ± 6	3 ± 2	73 ± 3
<hr/>			
SiSe_4			
$N_{\text{Si}}(\text{ES})$	$N_{\text{Si}}(\text{CS})$	$N_{\text{Si-Si}}$	$N_{\text{Se-Se}}$
29 ± 4	67 ± 6	4 ± 2	72 ± 3
<hr/> <hr/>			

sponding $\text{Ge}_x\text{Se}_{1-x}$ and $\text{Si}_x\text{Se}_{1-x}$ glassy systems,²³ are thereby identified by using FPMD methods. The fractions of *AA*, *AB*, and *BB* units found for $g\text{-GeSe}_4$ and $g\text{-SiSe}_4$ are indicative of a larger structural variability for $g\text{-SiSe}_4$ since the percentage of

$$AB(g\text{-GeSe}_4) > AB(g\text{-SiSe}_4),$$

$$BB(g\text{-GeSe}_4) < BB(g\text{-SiSe}_4),$$

and

$$AA(g\text{-GeSe}_4) < AA(g\text{-SiSe}_4).$$

This behavior is confirmed by the larger number of edge-sharing tetrahedra in $g\text{-SiSe}_4$, with these configurations being associated with more numerous *AA* connections (Table I). The degree of departure of $g\text{-SiSe}_4$ and $g\text{-GeSe}_4$ from the full *AB* model is consistent with the larger width of the intermediate phase window that is indicated experimentally for the case of silicon selenide glasses.²³

We note that our first-principles description of the atomic ordering does not rely on the use of any experimental result

except for the atomic density. The configurations were not obtained by using a structural refinement method, in which diffraction data are used to improve the model,⁵¹ and are therefore independent of the methods employed to manufacture the glasses used for the diffraction experiments.

V. CONCLUSIONS

In summary, the detailed atomic structure of two related but chemically distinct intermediate phase glasses has been investigated by using neutron-diffraction and first-principles molecular dynamics. Our approach is substantiated by the excellent agreement found between experiment and theory at the level of the total structure factor and total pair-correlation

function. Departures from a single floppy to stressed-rigid transition are related to the character of the atomic conformations, leading to structural differences with respect to a chemically ordered reference network of undefective AB_4 corner-sharing tetrahedra. Neutron-diffraction studies aimed at unraveling the details of the coordination environment through the evaluation of the partial structure factors^{17,41–43,52} appear very well suited to further substantiate this result.

ACKNOWLEDGMENT

We thank Piers Buchanan for help with the ISIS experiment.

-
- ¹W. Bresser, P. Boolchand, and P. Suranyi, *Phys. Rev. Lett.* **56**, 2493 (1986).
²P. Boolchand, *Phys. Rev. Lett.* **57**, 3233 (1986).
³X. Feng, W. J. Bresser, and P. Boolchand, *Phys. Rev. Lett.* **78**, 4422 (1997).
⁴D. Selvanathan, W. J. Bresser, and P. Boolchand, *Phys. Rev. B* **61**, 15061 (2000).
⁵Y. Wang, P. Boolchand, and M. Micoulaut, *Europhys. Lett.* **52**, 633 (2000).
⁶P. Boolchand, D. G. Georgiev, and B. Goodman, *J. Optoelectron. Adv. Mater.* **3**, 703 (2001).
⁷Y. Wang and K. Murase, *J. Non-Cryst. Solids* **326-327**, 379 (2003).
⁸P. Boolchand, X. Feng, and W. J. Bresser, *J. Non-Cryst. Solids* **293-295**, 348 (2001).
⁹P. Boolchand, P. Chen, M. Jin, B. Goodman, and W. J. Bresser, *Physica B* **389**, 18 (2007).
¹⁰M. T. M. Shatnawi, C. L. Farrow, P. Chen, P. Boolchand, A. Sartbaeva, M. F. Thorpe, and S. J. L. Billinge, *Phys. Rev. B* **77**, 094134 (2008).
¹¹I. Petri and P. S. Salmon, *Phys. Chem. Glasses* **43C**, 185 (2002).
¹²S. Hosokawa, *J. Optoelectron. Adv. Mater.* **3**, 199 (2001).
¹³S. Hosokawa, Y. Wang, J.-F. Bézar, J. Greif, W.-C. Pilgrim, and K. Murase, *Z. Phys. Chem.* **216**, 1219 (2002).
¹⁴R. W. Johnson, D. L. Price, S. Susman, M. Arai, T. I. Morrison, and G. K. Shenoy, *J. Non-Cryst. Solids* **83**, 251 (1986).
¹⁵Y. Wang, E. Ohata, S. Hosokawa, M. Sakurai, and E. Matsubara, *J. Non-Cryst. Solids* **337**, 54 (2004).
¹⁶D. Sharma, S. Sampath, N. P. Lalla, and A. M. Awasthi, *Physica B* **357**, 290 (2005).
¹⁷P. S. Salmon, *J. Non-Cryst. Solids* **353**, 2959 (2007).
¹⁸J. C. Phillips, *J. Non-Cryst. Solids* **34**, 153 (1979).
¹⁹M. F. Thorpe, *J. Non-Cryst. Solids* **57**, 355 (1983).
²⁰M. F. Thorpe, D. J. Jacobs, M. V. Chubynsky, and J. C. Phillips, *J. Non-Cryst. Solids* **266-269**, 859 (2000).
²¹M. Micoulaut, *Europhys. Lett.* **58**, 830 (2002).
²²M. Micoulaut and J. C. Phillips, *Phys. Rev. B* **67**, 104204 (2003).
²³A. Sartbaeva, S. A. Wells, A. Huerta, and M. F. Thorpe, *Phys. Rev. B* **75**, 224204 (2007).
²⁴M. J. Haye, C. Massobrio, A. Pasquarello, A. De Vita, S. W. de Leeuw, and R. Car, *Phys. Rev. B* **58**, R14661 (1998).
²⁵A. C. Hannon, *Nucl. Instrum. Methods Phys. Res. A* **551**, 88 (2005).
²⁶URL: www.isis.rl.ac.uk/disordered/Manuals/gudrun/Gudrun_manual_2006.pdf.
²⁷P. S. Salmon, S. Xin, and H. E. Fischer, *Phys. Rev. B* **58**, 6115 (1998).
²⁸S. Nosé, *Mol. Phys.* **52**, 255 (1984); W. G. Hoover, *Phys. Rev. A* **31**, 1695 (1985).
²⁹P. E. Blöchl and M. Parrinello, *Phys. Rev. B* **45**, 9413 (1992).
³⁰J. P. Perdew, J. A. Chevary, S. H. Vosko, K. A. Jackson, M. R. Pederson, D. J. Singh, and C. Fiolhais, *Phys. Rev. B* **46**, 6671 (1992).
³¹A. Dal Corso, A. Pasquarello, A. Baldereschi, and R. Car, *Phys. Rev. B* **53**, 1180 (1996).
³²C. Massobrio, A. Pasquarello, and R. Car, *Phys. Rev. Lett.* **80**, 2342 (1998).
³³C. Massobrio, A. Pasquarello, and R. Car, *J. Am. Chem. Soc.* **121**, 2943 (1999).
³⁴C. Massobrio, A. Pasquarello, and R. Car, *Phys. Rev. B* **64**, 144205 (2001).
³⁵C. Massobrio and A. Pasquarello, *Phys. Rev. B* **75**, 014206 (2007).
³⁶C. Massobrio and A. Pasquarello, *Phys. Rev. B* **77**, 144207 (2008).
³⁷M. Celino and C. Massobrio, *Phys. Rev. Lett.* **90**, 125502 (2003).
³⁸L. Giacomazzi, C. Massobrio, and A. Pasquarello, *Phys. Rev. B* **75**, 174207 (2007).
³⁹R. Azoulay, H. Thibierge, and A. Brenac, *J. Non-Cryst. Solids* **18**, 33 (1975).
⁴⁰F. Inam, M. T. Shatnawi, D. N. Tafen, S. J. L. Billinge, P. Chen, and D. A. Drabold, *J. Phys.: Condens. Matter* **19**, 455206 (2007).
⁴¹I. T. Penfold and P. S. Salmon, *Phys. Rev. Lett.* **67**, 97 (1991).
⁴²I. Petri, P. S. Salmon, and H. E. Fischer, *Phys. Rev. Lett.* **84**, 2413 (2000).
⁴³P. S. Salmon and I. Petri, *J. Phys.: Condens. Matter* **15**, S1509 (2003).
⁴⁴A. B. Bhatia and D. E. Thornton, *Phys. Rev. B* **2**, 3004 (1970).
⁴⁵The relationship between the three sets of partial structure factors commonly used (Faber-Ziman, Ashcroft-Langreth, and

- Bhatia-Thornton) can be found in Y. Waseda, *The Structure of Non-Crystalline Materials* (McGraw-Hill, New York, 1980).
- ⁴⁶P. S. Salmon, Proc. R. Soc. London, Ser. A **437**, 591 (1992).
- ⁴⁷C. Massobrio, M. Celino, and A. Pasquarello, Phys. Rev. B **70**, 174202 (2004).
- ⁴⁸F. H. M. van Roon, C. Massobrio, E. de Wolff, and S. W. De Leeuw, J. Chem. Phys. **113**, 5425 (2000).
- ⁴⁹I. Petri, P. S. Salmon, and H. E. Fischer, J. Phys.: Condens. Matter **11**, 7051 (1999).
- ⁵⁰D. N. Tafen and D. A. Drabold, Phys. Rev. B **71**, 054206 (2005).
- ⁵¹H. E. Fischer, A. C. Barnes, and P. S. Salmon, Rep. Prog. Phys. **69**, 233 (2006).
- ⁵²P. S. Salmon, R. A. Martin, P. E. Mason, and G. J. Cuello, Nature (London) **435**, 75 (2005).